Control of rare intense events in spatiotemporally chaotic systems

Viktor Nagy and Edward Ott
University of Maryland, College Park, Maryland 20742, USA
(Received 3 August 2007; revised manuscript received 15 October 2007; published 18 December 2007)

We address the problem of using feedback control for the purpose of suppressing rare intense events in spatially extended systems. As an example, we investigate the use of control to suppress turbulent spikes in the complex Ginzburg-Landau equation in the limit of small dissipation. We explore how information obtained by forecasting can be used to implement spatially and temporally localized control parameter changes and how control strength and cost are related to effectiveness in this framework. The effects of model error and imperfect state measurement are also considered.

DOI: 10.1103/PhysRevE.76.066206 PACS number(s): 05.45.Gg, 05.45.Jn

I. INTRODUCTION

There are numerous examples of rare intense events in spatiotemporal chaotic systems [1], some of which have great practical importance. Atmospheric events like tornados and hurricanes can be particularly harmful and capable of causing serious loss. Another example is the occurrence of large height ocean waves [2] (so-called rogue waves). An example of a nicely controllable laboratory model exhibiting rare intense event behavior is that of parametrically forced surface waves on water which intermittently produce high amplitude spatially localized upward jetting [3]. For cases in which such intense events are destructive, it would be highly desirable to find effective methods for suppressing them.

Synchronization and control of spatially extended systems has attracted considerable attention during the last 2 decades partly because of the broad range of its potential applications, see, e.g., Refs. [4–7]. The first approaches to control spatiotemporal chaos were extensions of the algorithm in Ref. [8]. Subsequently Pyragas suggested a delayed continuous feedback control method [9] which was extended to spatiotemporal systems to suppress turbulence in the complex Ginzburg-Landau equation [4] and to control chaos in an optical system by Lu *et al.* [6]. As simple models for spatially extended systems, coupled map lattice systems have attracted considerable attention where so-called "pinning control" techniques have been investigated [10,11]. In the context of low dimensional chaos, control for the suppression of rare intense events (e.g., associated with parameters putting the system slightly past a "crisis" [12]) has been addressed in Ref. [13].

The purpose of this paper is to address the problem of controlling rare intense events in spatiotemporally chaotic systems. We often refer to such rare intense events as "bursts." We take an approach in which we first forecast the future occurrence of an unwanted burst event in the uncontrolled system. We then use this information for planning a control to eliminate this burst event. We summarize the requirements of our control setup as follows.

(1) A good model of the system dynamics.

(2) Measurements of the state of the system.

(3) A means of using the previous two to predict the future system state and in particular the occurrence of bursts.

(4) Available control variables that can be physically changed to influence the system evolution.

(5) A strategy for deciding how to program these control variables.

Thus our considerations here are not applicable to examples of rare intense events (e.g., earthquakes) where the system is so complex that reliable prediction has so far proved unattainable. On the other hand, weather and hurricane prediction is rapidly advancing and may, in the future, provide an example where our considerations are of interest. For the case of hurricanes, one possibility [14] is to deposit surfactant on the ocean surface in the region of an incipient hurricane to reduce the evaporation that powers the storm. The purpose of our paper is to illustrate and examine the feasibility and limitations of burst elimination control for appropriate spatiotemporally chaotic systems. For this purpose we employ a specific simple model which will allow us to address many of the more basic issues raised by the above program. In particular, we use as our basic model system the complex Ginzburg-Landau (CGL) equation with parameter values chosen so that the equation exhibits large spatially and temporally localized bursts that occur in a highly intermittent manner.

As background, in Sec. II we discuss the properties of the uncontrolled CGL equation in the regime of interest. In Sec. III we consider a "perfect scenario" in which it is assumed that the following conditions hold.

(1) We are able to exactly sense the entire system state.

(2) We are in possession of an exact model for the system being controlled and we can integrate this model with arbitrarily fine precision.

By examining this perfect scenario we are able to address several issues illustrating the best possible results that could be expected. For example, how far do we need to predict into the future, and how does this prediction horizon influence the size and strength of the needed control? Can controls of fairly small size, if strategically applied and programmed, eliminate large, potentially catastrophic events? Can the control to eliminate a spatially localized burst itself be localized in space and time? We find that potentially favorable results can often be obtained. Thus the results from our perfect scenario tests motivate further study to investigate nonideal effects. This will be done in Sec. IV in which we consider the effects of the following practically important factors.

(1) Estimation of the current system state from *noisy* observations at a *finite* number of spatial locations.

(2) Model error (i.e., the model used to forecast bursts does not precisely correspond to the true dynamics of the system to be controlled).

In Sec. V we summarize our conclusions.

II. COMPLEX GINZBURG-LANDAU EQUATION AS A MODEL FOR RARE INTENSE EVENTS

The complex Ginzburg-Landau (CGL) equation,

$$\partial_t u = Ru - (\gamma - i\alpha)|u|^2 u + (\mu + i\beta)\nabla^2 u, \tag{1}$$

is a generic amplitude equation that describes the slow modulation of physical fields in space and time near the threshold of an instability (e.g., see Ref. [15]). It has been studied as a model for such diverse situations as fluid dynamics (Rayleigh-Bernard convection [16], Taylor-Couette flow [17], and Poiseuille flow [18]) and nonlinear chemical oscillation [19]. The CGL equation can also be viewed as a dissipative extension of the nonlinear Schrodinger (NLS) equation which corresponds Eq. (1) with R, γ, and μ set to zero. For real positive $(R, \gamma, \alpha, \mu, \beta)$ solutions of the CGL equation are global in time [20,21], while, in contrast, the NLS equation can exhibit finite-time singularities in which the field approaches infinity ("blow-up") at some point in space as the time approaches a singularity time from below [23–25]. Here we consider the CGL equation on a two-dimensional domain (denoted Ω) with periodic boundary conditions. Furthermore, we consider a parameter region where the CGL equation is close to the NLS limit:

$$\alpha = \beta = 40 \gg \gamma = R = \mu = 1. \tag{2}$$

In this regime the CGL solution intermittently develops high-amplitude, spatially localized, intense bursts [26–28] which can be considered as dissipative versions of the finite-time blow-up solutions of the NLS equation. Due to dissipation (nonzero γ and μ) the amplitude of these CGL bursts (in contrast to the NLS blow-up solutions) never reaches infinity [20,21]. We consider such CGL bursts as a generic model for rare intense events.

In our numerical solution of Eq. (1) we employ periodic boundary conditions on a square with side length $l=60$. We use a 512×512 grid and a second-order accurate operator splitting method in time (e.g., Ref. [22]) with adaptively changing time step. The accuracy of our numerical simulations is most restricted by the limited spatial resolution as bursts exhibit large amplitude variations within small distances. In order to check the accuracy of the selected method, we performed our numerical integration for finer resolutions in space and time and found good quantitative agreement between the results.

We start our numerical integration from random initial conditions and integrate the system forward in time until transients related to the initial conditions seem to be absent (i.e., the solution approaches the compact global attractor [21]). We use the resulting state (labeled $t=0$) as an initial condition for the following calculations. Figure 1 shows a snapshot of the spatial dependence of $|u|$ in a region containing a burst at the snapshot time. Figure 2 shows $|u|$ evaluated at the spatial location of the maximum of $|u|$ in Fig. 1 versus time. As seen in Fig. 2, this quantity initially fluctuates showing both increasing and decreasing behavior. Subsequently, when conditions are favorable to lead to formation of a burst, the amplitude starts to increase rapidly. When bursts finally reach their maximum amplitude, to within a good approximation, they are circularly symmetric around their maxima and differ only in an appropriate scaling,

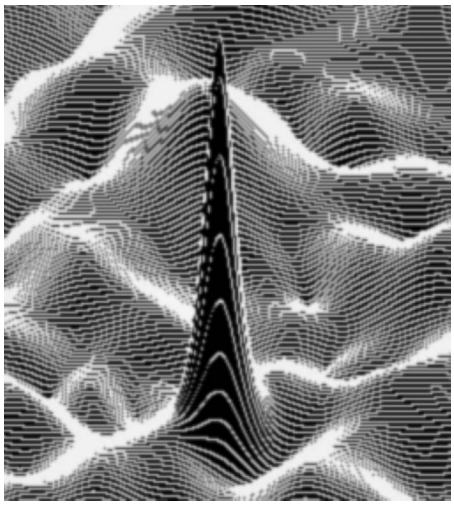

FIG. 1. Three-dimensional view of a CGL burst.

$$\frac{u'(r/|u'|_{\max})}{|u'|_{\max}} \simeq \frac{u(r/|u|_{\max})}{|u|_{\max}} e^{i\phi}, \tag{3}$$

where $u(r)$ and $u'(r)$ denote solutions of a CGL equation at the time where two independent bursts reach their amplitude, with r denoting the spatial distance from the burst maximum. Self-similarity first appears close to the spatial location of the maximum amplitude and, as the increase continues, extends to larger r. Thus, despite the complexity of the underlying system, we have to control objects that are becoming quite similar as they approach their maximum amplitudes. The observed approximate similarity of CGL bursts is inherited from the well-studied asymptotic self-similarity of the blow-up solutions of the NLS equation [29–31].

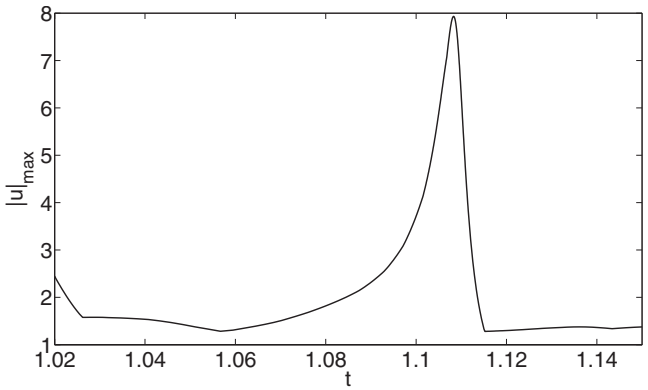

FIG. 2. $|u|_{\max}$ versus time for an individual burst. Solution of Eq. (1) with parameters as given in Eq. (2).

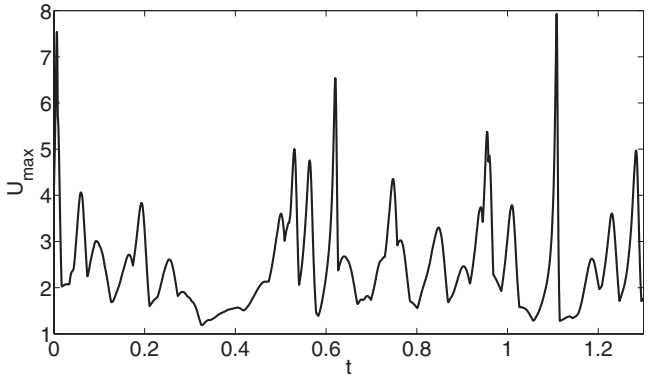

FIG. 3. $U_{\max}$ versus time for Eq. (1) with periodic boundary conditions on a square with side length $l=60$.

Figure 3 shows the global spatial maximum of the amplitude,

$$U_{\max} = \max_{x\in\Omega} |u(x,t)|, \tag{4}$$

as a function of time resulting from a typical numerical integration of Eq. (1) with parameters (2).

We note that for this simulation the spatially averaged amplitude over the periodic area Ω,

$$U_{\text{ave}}(t) = \frac{1}{|\Omega|}\int_{\Omega} |u(x,t)| d^2x, \tag{5}$$

is about $U_{\text{ave}} \simeq 0.3$ and fluctuates less than 10% with time. This average amplitude of ~ 0.3 is to be contrasted with the much larger values sometimes attained by $U_{\max}(t)$; e.g., the largest $U_{\max}$ in Fig. 3 is $U_{\max} \simeq 7.5$, and an integration somewhat longer yields a value of $U_{\max}$ above 13. Bursting also occurs on a very fast time scale; the usual time needed for a burst to develop from $|u|=1$ to $|u|_{\max}$ is typically smaller than 0.1. Integrating the solution for a sufficiency long time, we can determine the conditional empirical probability $P(v)$ of maximum burst amplitudes,

$$P(v) = \left[\frac{\text{No. of bursts with } (|u|_{\max} \geq v)}{\text{No. of bursts with } (|u|_{\max} \geq 1)}\right]. \tag{6}$$

Thus we consider the distribution only for those bursts whose maximum amplitude exceeds 1. $P(v)$ is shown in Fig. 4(a), and it illustrates that, although extremely high amplitudes occur frequently, because of their fast time scale, their contribution to the distribution is relatively small. As we will discuss later, these large amplitude bursts make a significant contribution to the overall average dissipation in the system. Figure 4(b) shows a log-linear plot of the same data as in Fig. 4(a). From its approximately linear form we see that $P(x) \sim \exp(-cx)$ for $x \in [2,10]$, i.e., $P(v)$ has an exponential event tail. For further details on statistics of the CGL equation see [26,32]. The characteristics of CGL bursts seen in Figs. 1–4 make them particularly suitable as a model for rare intense events in spatiotemporally chaotic systems.

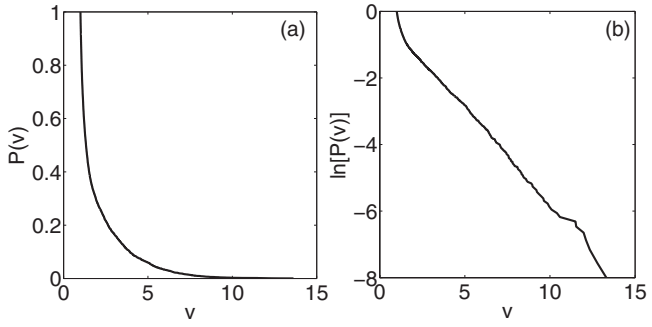

FIG. 4. $P(v)$ and $\ln(P(v))$ versus v. The distributions are calculated using a computer experiment of duration $t=40$ for Eq. (1) with parameters as given in Eq. (2) [No. of bursts with $(|u|_{\max} \geq 1) \simeq 5000$].

III. PERFECT CONTROL SCENARIO

We assume that in real physical situations the most violent rare events are of primary concern. Thus in our model experiments using the CGL equation our intention is to deal with the highest amplitude bursts. We choose an amplitude u_c past which we assume a burst becomes particularly destructive. Thus we wish our control to prevent bursts of amplitude larger than u_c, which we suppose to be much larger than the average amplitude, $u_c \gg U_{\text{ave}}$. We refer to u_c as the *control limit*.

Assume that at any given time t_0 we have an estimate of the system state $u_e(x,t_0)$ and a model M'_τ for advancing the uncontrolled system state forward in time by the amount τ. Then our forecast is

$$u_f(x,t) = M'_\tau[u_e(x,t_0)], \quad t > t_0. \tag{7}$$

We note that in general $u_e(x,t_0)$ may differ from the true system state $u(x,t_0)$ [i.e., $|u_e(x,t_0) - u(x,t_0)| > 0$] and M'_τ may differ from the true system dynamics, M_τ [i.e., $|M'_\tau[u(x,t_0)] - M_\tau[u(x,t_0)]| > 0$]. In the ideal case, or perfect scenario, we assume that such differences are absent. In particular $u(x,t_0) = u_e(x,t_0)$, and $M_\tau = M'_\tau$, where M_τ and M'_τ are integrations of Eq. (1) using the same numerical algorithms (including space and time gridding) for both M_τ and M'_τ. (In Sec. IV we consider what happens when these ideal conditions do not hold.)

A. Control strategy

We introduce the following definitions.

(1) Let $C_r(x)$ be the circular region in the doubly periodic domain Ω that is within a distance r of the point x; i.e., if y is in $C_r(x)$, then

$$[\min(|x_1 - y_1|, l - |x_1 - y_1|)]^2 + [\min(|x_2 - y_2|, l - |x_2 - y_2|)]^2 < r^2 \tag{8}$$

where l is the periodicity length and $(x_1,x_2),(y_1,y_2)$ are the coordinates of x and y.

(2) Define a *burst* b as a local space-time maximum of $|u|$ that satisfies $|u| > u_c$ and denote its coordinates by (x_b,t_b),

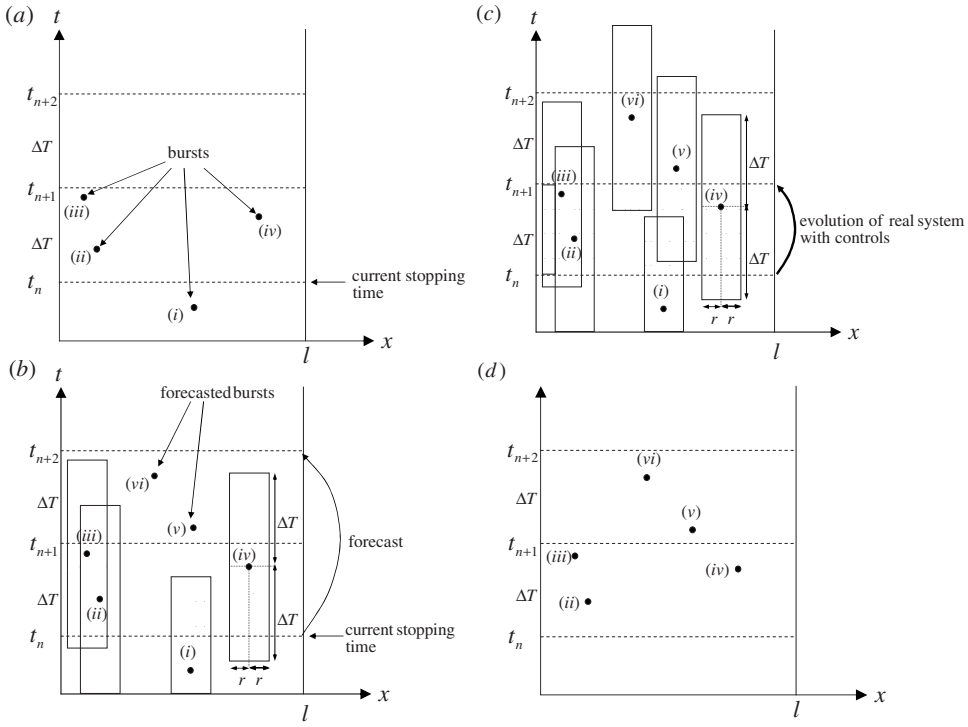

FIG. 5. Systematic illustration of the control procedure.

where x_b and t_b are the spatial location and time of burst b.

(3) Define *cycle times* $t_n = t_0 + n\Delta T$, where t_0 is the time at which we start our control procedure, n is a positive integer, and ΔT is a fixed time interval.

(4) Define a list L_n of burst coordinates (where, as explained below, n corresponds to the time interval t_n to t_{n+1}).

(5) The act of making a forecast is defined as taking an estimate of the current state of the system, integrating a copy of this current state forward in time via a forecasting system model, and monitoring the result.

Our control procedure is as follows.

(1) Start with $n=0$ and the list L_0 empty.

(2) At time t_n estimate the current state of the system to be controlled.

(3) Using the state estimate $u_e(x,t_n)$ obtained in step 2, do a forecast to determine the burst coordinates that occur between cycle times t_{n+1} and t_{n+2}. For the purpose of making this forecast, the forecast model is integrated with control applied at (x,t) if x is in $C_r(x_b)$ and $t \in [t_b - \Delta T, t_b + \Delta T]$, where (x_b,t_b) is one of the entries of the list L_n.

(4) Add the newly determined (step 3) burst coordinates to the list L_n.

(5) As the real system (as distinct from the forecast model) evolves from the time t_n to the time t_{n+1}, apply control at those points x and times t satisfying $x \in C_r(x_b)$, $t \in [t_b - \Delta T, t_b + \Delta T]$ where (x_b,t_b) are bursts on the list L_n.

(6) Remove burst coordinates (x_b,t_b) from the list L_n, if $t_b < t_{n-1}$.

(7) Increase n by one and go to step 2.

We emphasize that at cycle time t_n we determine bursts in the time interval $[t_{n+1},t_{n+2}]$ (see step 3) not in $[t_n,t_{n+1}]$. The reason why we choose sequencing this way is that we found it to be more effective compared to other types of sequencings that we have tried. A reason for this is that control, particularly if it is limited in strength, needs a sufficient amount of time to take effect, and our setup specified above provides us with at least ΔT time units before the occurrence of a burst. (Our control algorithm also implies that there is no control between t_0 and t_1.)

Figure 5 gives a schematic illustration of the steps involving the list L_n and its updating. For the purpose of this schematic, we represent the two-dimensional circular region $C_r(x)$ [Eq. (8)] as a one-dimensional interval; i.e., as $[x-r,x+r]$, where x denotes the (schematically one-dimensional) spatial location of the burst. Figure 5(a) shows the situation at the end of step 7 (i.e., before application of step 2) in which the only points on the list L_n are those that were on the list L_{n-1} and whose time coordinate is greater than t_{n-1}. As illustrated in Fig. 5(b), the forecast made in step 3 is done with the control applied in the shaded regions. The resulting newly forecasted bursts with $t_{n+1} \le t_b \le t_{n+2}$ are labeled (v) and (vi) in this figure. As illustrated in Fig. 5(c), the bursts determined in step 3 [bursts (v) and (vi)] are added to the list (step 4), and the real system is controlled in the shaded region as it evolves from time t_n to time t_{n+1} (step 5). Figure 5(d) shows those points that are still on the list after step 6 (in which bursts whose time coordinates smaller than t_n [labeled (i) in Figs. 5(a)–5(c)] are removed from the list).

B. Numerical experiments

In all our numerical experiments we use the parameter α appearing in the CGL equation, Eq. (1), as our control variable. In a real experiment this would be analogous to assuming that there is some physical means by which α can be changed through external intervention. In particular, our control consists of lowering the value of α. That is, with reference to Fig. 5(c) we replace α in Eq. (1) by a value $\alpha' < \alpha$

for those (x,t) in the shaded region of Fig. 5(c). The specific form of the control that we have chosen to implement depends on two positive parameters m, u_c. If $|u(x,t)|<1$ for $x \in C_r(x_b)$ then we keep α unchanged. On the other hand, if $|u(x,t)|>1$ for $x \in C_r(x_b)$, then we lower the value of α to α',

$$\alpha'(x,t) = \frac{\alpha}{1+m[|u(x,t)|-1]} \quad \text{for } |u(x,t)|>1, \tag{9}$$

$$\alpha'(x,t) = \alpha \quad \text{for } |u(x,t)| \le 1. \tag{10}$$

The parameter m and can be regarded as characterizing the strength of the control, with $m=0$ corresponding to no control. Our choice is somewhat arbitrary and efficient control can also be achieved by using other choices [33].

Our spatially and temporarily localized changes in the control parameter α will modify the system dynamics, and the system consequently evolves differently than predicted in the forecast stage. This difference could conceivably lead to bursts that were not predicted during the forecast or to nonnegligible changes in the timing and position of those bursts for which we already have information. This difficulty can be overcome by choosing ΔT sufficiently small that the difference due to control will not compromise our predictions. Choosing ΔT too small, however, can leave us with insufficient time to make significant changes in the amplitudes. We have found that the best selection of ΔT does not depend strongly on the particular choice of the parameters m, u_c for their tested ranges in our numerical experiments. Thus in what follows we use a constant value, namely $\Delta T=0.1$.

Considering the entire periodic box of our simulation Ω, we define the "expense" of control as the fractional space-time averaged change in α:

$$\delta = \frac{1}{|\Omega|T}\int_0^T dt \int_\Omega \frac{|\alpha'(x,t)-\alpha|}{\alpha} d^2x, \tag{11}$$

where $t=0$ corresponds to the time at which we start monitoring and controlling bursts, and $t=T$ is the time at the end of our computer experiment. We will regard our method as effective if we can significantly lower the probability of bursts with amplitudes exceeding u_c at low expense δ. We use $r_0=2$ in all cases, as we have found that the results are insensitive to deviations from this value. With ΔT and r_0 fixed, we choose a "standard case" for the remaining two parameters,

$$m^{sd} = 1/4, \quad m_c^{sd} = 3. \tag{12}$$

This standard case serves as a point of reference for exploring the effects of varying m, u_c. In particular, we will change the value of one of the parameters, e.g., m, while fixing the other at its standard value, e.g., $u_c = u_c^{sd}$. For each such selection we determine the time averaged expense of control δ, and the empirical probability $P(v)$ [$P(v)$ is shown in Fig. 4 in the uncontrolled case].

We performed a series of numerical experiments where we calculate $P(v)$ using data collected from experiments with increasing durations of time $t=20$, 40, and 80 to determine the rate of convergence. We found that the results for $t=40$ and 80 are in good agreement. Therefore we chose the time of integration to be $t=40$ in all perfect scenario cases. Using $P_0=2\times10^{-4}$ we can also define the "effective largest amplitude" that the controlled system reaches as $U(P_0)$,

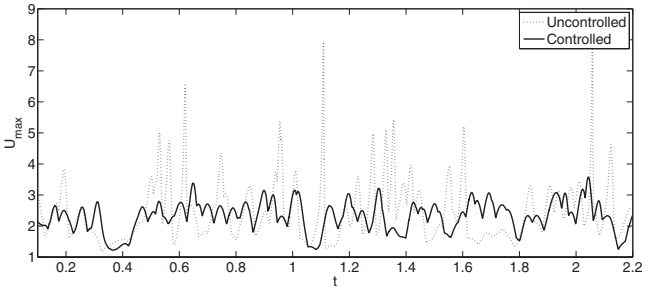

FIG. 6. $U_{\max}$ versus time without control (dotted curve) and with control (solid curve) using the standard control parameters given in Eq. (12).

$$P(U(P_0)) = P_0. \tag{13}$$

We numerically define this $U(P_0)$ to be the "effective upper limit" of $|u|$ with our control. A typical time series of $U_{\max}(t)$ versus t for a controlled run using our standard parameter set is shown in Fig. 6 by the full black curve. For comparison an uncontrolled run is also shown in this figure as the dotted curve. Large bursts are apparently strongly suppressed by the control. This later conclusion is also reflected in the substantially lower value obtained for $U(P_0)$ in the controlled case, $U(P_0)=4.7$, as compared to $U(P_0)=12.5$ in the uncontrolled case. It is significant that this improvement is obtained at a relatively small expense, $\delta=2.7\times10^{-4}$. The reason why the control expense can be kept at such a low level is because the area where burst amplitudes exceed the control limit u_c is relatively small compared to the system size and because the burst events ($|u|>u_c$) are of short duration.

Imposing control on the system will result in its departure from its original dynamics which is accompanied by an observable quantitative change in the space-time average of $|u|^2$ denoted $\langle|u|^2\rangle$. Starting with a long uncontrolled run and then activating our control, we observe that after the initial transients relax, the value $\langle|u|^2\rangle$ settles down to a new level that

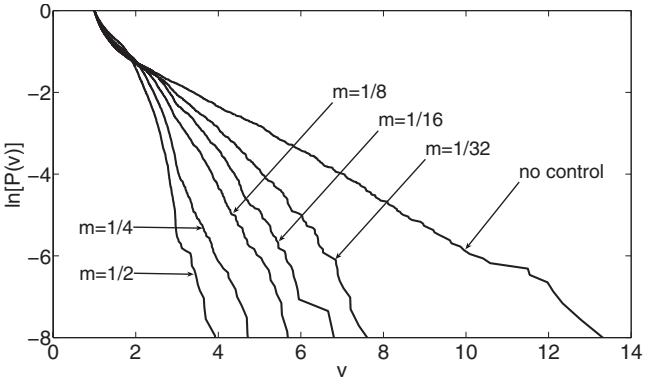

FIG. 7. $\ln(P(v))$ versus v for $m=0$, 1/32, 1/16, 1/8, 1/4, and 1/2 with $u_c=u_c^{sd}$.

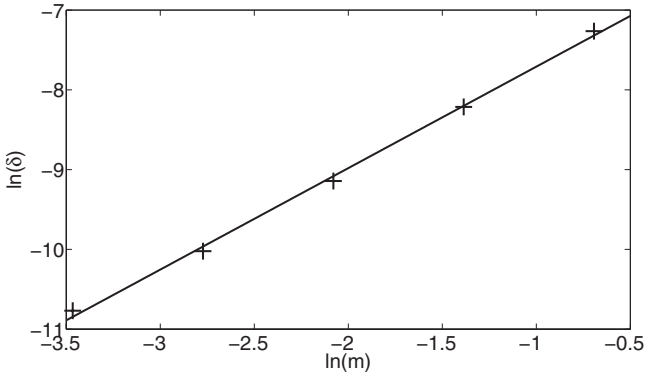

FIG. 8. Expense of control $\ln(\delta)$ as a function of $\ln(m)$ with $u_c=u_c^{sd}$.

is somewhat *larger* than before the control was activated. We attribute this effect to the fact that the amount of dissipation in a burst event increases with its amplitude. Thus the total dissipation due to bursts can be much larger than would be expected on the basis of the relatively small fraction of the available space time in which they are active. We believe that this lowering of the burst contribution to the space-time average dissipation is what causes the increase of $\langle|u|^2\rangle$. With our "standard case" parameter set we observed a control induced increase of $\langle|u|^2\rangle$ from a value of 0.13 to 0.16.

C. Dependence on the control parameters m, u_c

A comparison of $P(v)$ for different m values is shown in Fig. 7. Figure 8 shows the expense of control δ as a function of m on a log-log plot. We can see that the dependence of δ on m is approximately a power law,

$$\delta(m) \simeq am^b \tag{14}$$

with $a \simeq 1.6\times 10^{-3}$, $b \simeq 1.27$. These figures illustrate that increasing m decreases the probability of high amplitude bursts for an increasing expense δ. We also notice that, while we suppress high intensity bursts, there is an increased probability $P(v)$ for the ones whose amplitudes are below the control limit u_c. Figure 9 shows the "effective largest amplitude" $U(P_0)$ as a function of m on a log-log plot. The parameters of the power law dependence,

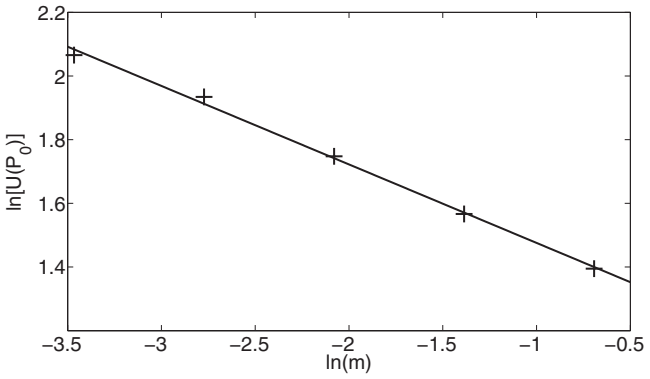

FIG. 9. $\ln(U(P_0))$ versus $\ln(m)$ with $u_c=u_c^{sd}$.

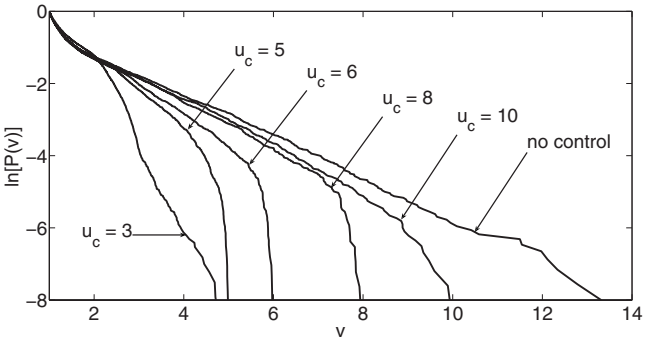

FIG. 10. Distribution $P(v)$ for $u_c=3,\ 5,\ 6,\ 8,\ 10,\ \infty$ with $m=m^{sd}$.

$$U(P_0) \simeq cm^{-d}, \tag{15}$$

are $c \simeq 3.42$, $d \simeq 0.25$. Referring to Fig. 10, we see that variation of the control limit u_c does not significantly change the effective largest amplitude $U(P_0)$ provided that $u_c \leq U(P_0)^{sd} \simeq 4.3$ where $U(P_0)^{sd}$ denotes $U(P_0)$ with our standard selection of parameters. However, as we increase u_c above $U(P_0)^{sd}$ the effective largest amplitude will no longer be limited by the strength of control (m) but by u_c, and in this case we have $U(P_0) \simeq u_c$. While u_c does not effect $U(P_0)$ as u_c is reduced below $U(P_0)^{sd}$, it nevertheless causes δ to rise, as shown in Fig. 11 on a log-linear plot. We get the approximately exponential dependence,

$$\delta(m) \simeq ge^{-hu_c} \tag{16}$$

with parameters $g \simeq 1.57\times 10^{-3}$, $h \simeq 0.6$.

Finally, in order to illustrate the benefit of our forecast driven approach, we consider what happens when we apply the controls (9) and (10) everywhere and for all times (i.e., not just in the forecast-determined shaded regions of Fig. 4). Generally, we find that to achieve a similar level of burst suppression, not making use of forecasts leads to much greater cost. For example, using $m=1/16$ and applying Eq. (9) for all x and t suppresses bursts with $|u|_{\max} \geq 7$ at a cost $\delta \simeq 10^{-4}$. In contrast, using a forecast-based method with the parameters $m=1/16$, $u_c=7$ the cost is more than 20 times less that without forecast.

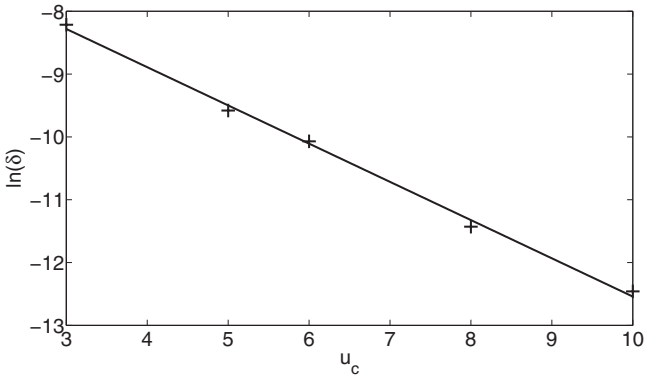

FIG. 11. δ versus u_c with $u_c=u_c^{sd}$.

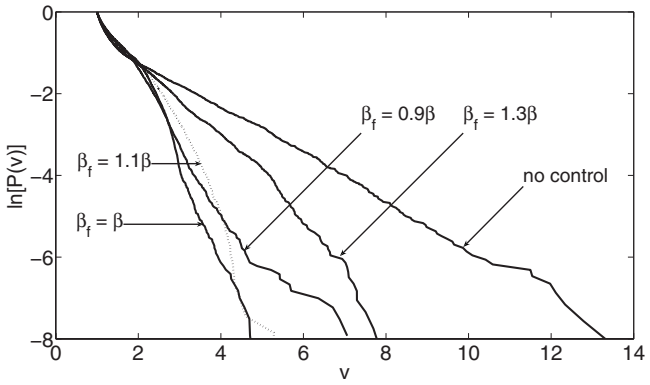

FIG. 12. Comparison of perfect and imperfect model scenarios.

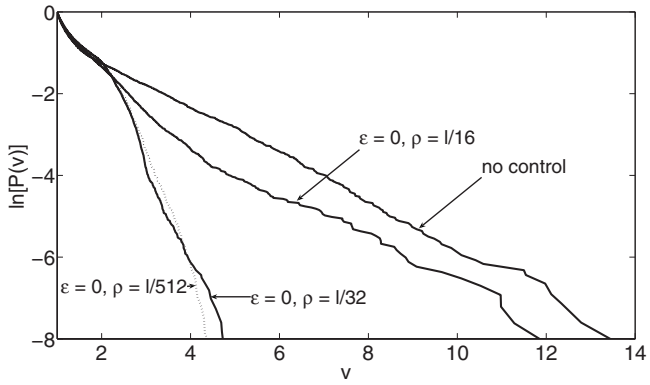

FIG. 13. Comparison of $P(v)$ for the standard control parameters (12) for different observation densities, with $\rho=l/512$, $l/32$, and $l/16$.

IV. IMPERFECT CONTROL SCENARIO

In the previous section we implemented our control strategy for the case in which we possess a perfect model of the controlled system and we are able to sense the state of the system with arbitrary precision. In any real situation, however, these ideal conditions will not be met. When implementing forecasting in practice, one typically estimates the state of the system using noisy observations made at a limited number of spatial locations and makes forecast predictions using this estimate as the initial condition in the forecast model integration. In addition to the limitations imposed by the accuracy and limited number of measurements, errors in the forecast model also contribute significantly to prediction inaccuracy. If a control strategy is to be applied to practical situations, it has to show sufficient robustness under less than perfect conditions. In this section we investigate the effects both of an imperfect model and of imperfect state estimation using our standard control parameters (12).

A. Imperfect model

To assess the effect of using an imperfect forecasting system model we use Eq. (1) but with an incorrect value of the parameter β denoted β_f for our forecast model. For this purpose we will assume that we can determine the initial conditions with arbitrary precision, so that the only source of error is our imperfect model. We find that, using the imperfect forecast model in our control procedure, the maximum amplitude of bursts is rather sensitive to variations of β_f while the accuracy of the predicted burst time and location remains good. Figure 12 shows a comparison of $P(v)$ for the uncontrolled and controlled systems. In the controlled case we plotted the results both for the perfect $\beta_f=\beta$ and imperfect model scenarios $\beta_f=0.9\beta$, 1.1β, and 1.3β. The apparent difference in $P(v)$ between the cases $\beta_f=1.1\beta$ and $\beta_f=0.9\beta$ is partly due to the fact that for $\beta_f>\beta$ the predicted amplitudes are larger than for $\beta_f=\beta$ and similarly a selection of β_f below β results in a decrease of the predicted height of bursts. As a consequence, for $\beta_f<\beta$, it is more likely that the predicted amplitude is smaller than the control limit u_c and that it remains unnoticed and uncontrolled despite being above u_c in the perfect model. Our results illustrate that, in spite of substantial error in one of the parameters of Eq. (1), the method still delivers significant suppression of unwanted bursts at reasonably low expense: $\delta=1.9\times10^{-4}$ for $\beta=1.1\beta$ and $\delta=3.3\times10^{-4}$ for $\beta=0.9\beta$.

B. Imperfect state estimation

We implement our imperfect state estimation scenario by placing a uniformly spaced sparse square "observational grid" on the entire periodic box of our simulation Ω with the observational grid points being our measuring locations. We define a measurement location density ρ as the distance between our measurement points in our observational grid (recall that our model uses a 512×512 grid on a periodic box of side length $l=60$). Simulated measurements at these locations are "observed" at the discrete "cycle times" $t_n=t_0+n\Delta T$, with n an integer, and measurements are generated by adding noise to the "true" value of u at each observation point. The noise simulates measurement error and is taken to be $\epsilon\sqrt{\langle|u|^2\rangle_0}(r_r+ir_i)$, where $\langle|u|^2\rangle_0$ denotes the mean squared time-space average of u in the absence of control, r_r and r_i are real, zero mean, independent, Gaussian random variables with variance one, and ϵ is a parameter characterizing the strength of the noise. We then reconstruct the system state at each "cycle time" using the Whittaker-Shannon sampling theorem in two dimensions. Prerequisites for avoiding the effect of aliasing with this method are that the signal be band limited and that the sampling rate be at least twice the bandwidth. As observed both numerically and verified theoretically [34], at sufficiently large wave numbers, the spatial Fourier coefficients of solutions of the CGL equation decay exponentially with increasing wave number. From our numerical investigations, we find that this exponential decay is also valid for the controlled system and that the assumption that the system is band limited is a good approximation. If we denote our sample points by $u[i,j]$, the reconstructed state by $u(x,y)$, and the sampling grid by $G_L=\{(iL,jL)|i,j\in0,\ldots,512/L\}$, where $L=512\times\rho/l$, then the Whittaker-Shannon interpolation formula yields the following estimate for the reconstructed system state:

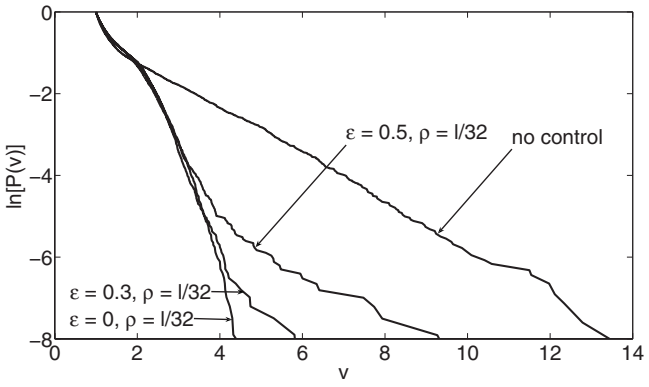

FIG. 14. Comparison of $P(v)$ for the standard control parameters (12) for different noise levels ϵ with $\rho=l/512$ and $l/32$.

$$u(x,y) = \sum_{(i,j)\in G_L} u[i,j]\frac{\sin[\pi(x-iL)/L]\sin[\pi(y-jL)/L]}{\pi^2(x-iL)(y-jL)/L^2}.$$

We found that this approximation gives good results for $\rho=l/32$ with the exception of locations where the amplitude is large (i.e., near bursts). A significant point is that, even though $\rho=l/32$ is not fine enough to resolve high amplitude bursts, it can still be used to accurately predict such bursts. This is because the initial conditions leading to a burst are much smoother than the burst itself, and it is only such initial conditions that we need to approximate in order to make our predictions. Comparison of $P(v)$ for controlled runs with different values of the observation density ρ are shown in Fig. 13 for $\epsilon=0$ (no observational noise). Results comparing the effect of different noise levels for $\rho=l/512$ and $l/32$ are shown in Fig. 14. Figure 13 indicates that the observation density $\rho=l/32$ without noise gives results that are somewhat worse than in the $\rho=l/512$ case, while $\rho=l/16$ is too sparse and gives only slight improvement over the uncontrolled system. Figure 14 indicates that increase of observational noise ϵ makes control increasingly less effective as shown for $\epsilon=0.3,0.5$.

V. CONCLUSION

In this paper we have investigated an approach to the control of rare intense events in spatiotemporally chaotic systems. The approach has several prerequisites.

(1) A sufficiently accurate model of system dynamics.

(2) Access to measurements of the system state that are of sufficient accuracy and spatial and temporal resolution.

(3) The ability to physically make local control perturbations to the system.

Given that these prerequisites are satisfied, our numerical experiments suggest that it may, in some cases, be feasible to effectively control physical systems exhibiting rare intense events at low expense. In particular, we have shown how the information obtained from a forecast can be applied to formulate and implement spatially and temporally localized control. This is to be contrasted with previous work where spatiotemporal chaos was controlled either globally [4,6,35] or locally with controllers located at fixed spatial locations, e.g., [36,37]. Furthermore, while several studies, e.g., [4,6,35,37], focused on forcing the controlled system to a nonchaotic region, e.g., toward plane wave solutions, our goal is not to significantly eliminate the chaotic nature of the dynamics, but rather to eliminate only its potentially most harmful part. This feature results in a potentially cost efficient control. We have found that time sequencing of control is a key issue for implementation of our control strategy, and we have investigated how control strength and cost are related to effectiveness. Moreover, model error and imperfect state measurement can impose important limitations.

We emphasize that our results may be limited in their applicability because of the simple "toy model" we have employed [the CGL equation, Eq. (1)], and that many additional issues can arise when a program of this type is attempted for a real physical system. We nevertheless hope that our results in this paper may provide some useful insight to real applications.

ACKNOWLEDGMENTS

We thank P. N. Guzdar for advice on the numerical solution of the complex Ginzburg Landau equation and C. D. Levermore for useful discussions. This work was supported by the Office of Naval Research (Physics) and by the National Science Foundation (Grants No. PHY 0456240 and No. ATM 034225).

[1] E. Events, in *Nature and Society*, edited by S. Albeviro, V. Jentsh, and H. Kantz (Springer-Verlag, Berlin, 2006).
[2] A. R. Osborne, M. Onorato, and M. Serio, Phys. Lett. A **275**, 386 (2000).
[3] E. J. Boettcher, J. Fineberg, and D. P. Lathrop, Phys. Rev. Lett. **85**, 2030 (2000).
[4] D. Battogtokh and A. Mikhailov, Physica D **90**, 84 (1996); D. Battogtokh and A. Mikhailov, *ibid.* **106**, 327 (1997).
[5] R. J. Wiener, D. C. Dolby, G. C. Gibbs, B. Squires, T. Olsen, and A. M. Smiley, Phys. Rev. Lett. **83**, 2340 (1999).
[6] W. Lu, D. Yu, and R. G. Harrison, Phys. Rev. Lett. **76**, 3316 (1996); W. Lu, D. Yu, and R. G. Harrison, *ibid.* **78**, 4375 (1997).
[7] R. Roy, T. W. Murphy, T. D. Maier, Z. Gills, and E. R. Hunt, Phys. Rev. Lett. **68**, 1259 (1992).
[8] E. Ott, C. Grebogi, and J. A. Yorke, Phys. Rev. Lett. **64**, 1196 (1990).
[9] K. Pyragas, Phys. Lett. A **170**, 421 (1992).
[10] H. Gang and Qu Zhilin, Phys. Rev. Lett. **72**, 68 (1994).
[11] R. O. Grigoriev, M. C. Cross, and H. G. Schuster, Phys. Rev. Lett. **79**, 2795 (1997).
[12] C. Grebogi, E. Ott, and J. A. Yorke, Physica D **7**, 181 (1983).
[13] W. Yang, M. Ding, A. Mandell, and E. Ott, Phys. Rev. E **51**, 102 (1995); V. In, M. L. Spano, J. D. Neff, W. L. Ditto, S.

Daw, K. D. Edwards, and K. Nyguyen, Chaos **7**, 605 (1997).Although these papers consider the suppression of a boundary crisis event, they also clearly apply directly to suppression of intermittent bursts, i.e., "rare intense events" associated with interior crises.

[14] J. Katz, Phys. Today **60**, 13 (2007); K. Emanuel, *ibid.* **60**, 13 (2007); R. Simpson and J. Simpson, Trans. N. Y. Acad. Sci. **28**, 1045 (1966).

[15] T. Bohr, M. H. Jensen, A. Vulpiani, and G. Paladin, *Dynamical Systems Approach to Turbulence* (Cambridge University Press, Cambridge, England, 2005), Chap. 5.

[16] A. C. Newell and J. A. Whitehead, J. Fluid Mech. **38**, 279 (1969).

[17] G. Ahlers and D. S. Cannell, Phys. Rev. Lett. **50**, 1583 (1983).

[18] K. Stewartson and J. T. Stuart, J. Fluid Mech. **48**, 529 (1971).

[19] Y. Kuramoto, *Chemical Oscillations, Waves and Turbulence* (Series in Synergetics Vol. 19) (Springer, New York, 1984).

[20] M. Bartuccelli, J. D. Gibbon, and M. Oliver, Physica D **89**, 267 (1996).

[21] A. Mielke, Physica D **117**, 106 (1998).

[22] M. Gabbay, E. Ott, and P.N. Guzdar, Physica D **118**, 371 (1998).

[23] M. J. Landman, G. C. Papanicolaou, C. Sulem, and P. L. Sulem, Phys. Rev. A **38**, 3837 (1988).

[24] B. J. LeMesurier, G. C. Papanicolau, C. Sulem, and P. L. Sulem, Physica D **32**, 210 (1988).

[25] G. Fibich and G. C. Papanicolaou, Phys. Lett. A **239**, 167 (1998).

[26] C. D. Levermore and D. R. Stark, Phys. Lett. A **234**, 269 (1997).

[27] R. E. Wilson, Physica D **112**, 329 (1998).

[28] B. P. Luce and C. R. Doering, Phys. Lett. A **178**, 92 (1993).

[29] G. Fibich and D. Levy, Phys. Lett. A **249**, 286 (1998).

[30] F. Merle and P. Raphael, Commun. Math. Phys. **253**, 675 (2005).

[31] F. Merle and P. Raphael, Invent. Math. **156**, 565 (2004).

[32] J. W. Kim and E. Ott, Phys. Rev. E **67**, 026203 (2003).

[33] In addition to control by modifying an intrinsic parameter of the system (e.g., our discussion of changing the parameter α), one might also envision adding an *externally applied* "control force" $f(x,t)$ to the right-hand side of Eq. (1) with the intrinsic system unchanged. We note, however, that our changing of α can also be viewed as an external force control with $f(x,t)$ chosen to be $i\alpha(\alpha'(x,t)-\alpha)|u|^2u$. Other choices for the control force $f(x,t)$ might, e.g., utilize an added nonlinear dissipation [such as $-m(x,t)|u|^\sigma u$ with $\sigma=2,3,\ldots$] or an added dispersion [such as $ip(x,t)\nabla^{2n}u$ with $n=1,2,\ldots$]. We have tried some of these alternative forms for the control and found that they can also perform well when used in our forecast driven control scenario illustrated in Fig. 5.

[34] A. Doelman and E. S. Titi, Numer. Funct. Anal. Optim. **14**, 299 (1993).

[35] R. Montagne and P. Colet, Phys. Rev. E **56**, 4017 (1997).

[36] L. Junge and U. Parlitz, Phys. Rev. E **61**, 3736 (2000).

[37] S. Boccaletti, J. Bragard, and F. T. Arecchi, Phys. Rev. E **59**, 6574 (1999).